Accepted Manuscript

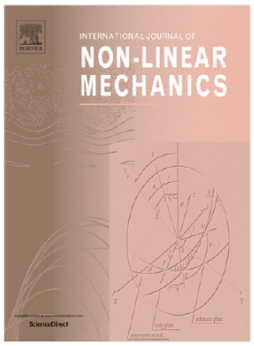

Analytical solutions for dynamics of dual-spin spacecraft and gyrostat-satellites under magnetic attitude control in omega-regimes

Anton V. Doroshin

PII: S0020-7462(17)30184-1
DOI: http://dx.doi.org/10.1016/j.ijnonlinmec.2017.08.004
Reference: NLM 2890

To appear in: *International Journal of Non-Linear Mechanics*

Received date : 9 March 2017
Revised date : 18 August 2017
Accepted date : 19 August 2017

Please cite this article as: A.V. Doroshin, Analytical solutions for dynamics of dual-spin spacecraft and gyrostat-satellites under magnetic attitude control in omega-regimes, *International Journal of Non-Linear Mechanics* (2017), http://dx.doi.org/10.1016/j.ijnonlinmec.2017.08.004

Analytical Solutions for Dynamics of Dual-Spin Spacecraft and Gyrostat-Satellites under Magnetic Attitude Control in Omega-Regimes

ANTON V. DOROSHIN

Space Engineering Department
Samara National Research University

Moskovskoe shosse 34, Samara, Russian Federation 443086
doroshin@ssau.ru; doran@inbox.ru

Abstract: - The attitude dynamics of a dual-spin spacecraft (a gyrostat with one rotor) with magnetic actuators attitude control is considered in the constant external magnetic field at the presence of the spacecraft's own magnetic dipole moment, which is created proportionally to the angular velocity components (this motion regime can be called as "the omega-regime" or "the omega-maneuver"). The research of the dual-spin spacecraft angular motion under the action of the magnetic restoring torque is fulfilled in the generalized formulation close to the classical mechanics' task of the heavy body/gyrostat motion in the Lagrange top. Analytical exact solutions of differential equations of the motion are obtained for all parameters in terms of elliptic integrals and the Jacobi functions. New obtained analytical solutions can be classified as results developing the classical fundamental problem of the rigid body and gyrostat motion around fixed point. The technical application of the omega-regime to the angular reorientation of the spacecraft longitudinal axis along the angular momentum vector is considered.

Key-Words: Spacecraft; Satellite; Gyrostat; Dual-Spin Spacecraft; Rigid Body Dynamics; Explicit Exact Solutions; Elliptical Integrals; Jacobi Elliptic Functions; Generalization; Lagrange Top; Omega-Regime

Introduction

An analytical investigation of the angular motion of rigid bodies systems together with its practical applications in the field of the attitude dynamics of spacecraft/satellites is one of the important actual scientific problems of the fundamental mechanics and the space flight dynamics, including classical tasks of the rigid body angular motion [1, 2], modern developments of these classical tasks with applications [3-7], as well as the rigid bodies and spacecraft regular and chaotic dynamical aspects [8-18]. As it is well known, analytical solutions for the system dynamical parameters allow to completely describe the system motion and to predict its time-evolutions and, moreover, analytical solutions/dependencies can be used for the parametrical synthesis of the spacecraft (SC) dynamics.

In this work the analytical solutions for the motion dynamics of the small SC (micro-/nano-satellites) with a magnetic control system are obtained. Besides the magnetic actuators (such as magnetic coils and/or torque rods), the SC investigated in the research contains one coaxial rotor/reaction-wheel with its own constant longitudinal angular momentum (Δ), so it is possible to consider the SC as the dual-spin spacecraft (DSSC) with the magnetic attitude control. The DSSC motion is considered in the constant external magnetic field. The own dipole moment of the DSSC is created by the magnetic attitude control system in the form proportional to the angular velocity components (this motion mode can be called as "the omega-regime"). The constancy of the external magnetic field in this research is conditioned by the consideration of the angular motion of the DCCS

at the orbital motion of its center mass along the short segment of the orbit, when the vector of the magnetic induction of the geomagnetic field practically does not change. Also in this research the absence of the gravitational torque is assumed, as differences among the values of the principal moments of inertia are usually small for micro-/nano- spacecraft.

The interaction between the external magnetic field and the DSSC own magnetic dipole moment generates the external torque affecting the attitude dynamics, that was studied in numerous publications with different formulations, for example [11-25]. As it is presented in previous works dedicated to the theme of SC dynamics with magnetic actuators [11-16], the control of the SC angular motion can be implemented with the help of changing the value of the SC own magnetic dipole moment (its components on the SC connected axis), which is created by magnetic coils/rods, and which interacts with the geomagnetic field. The possible control laws can use the information about the current angular parameters (the Euler angles, quaternions, the angular velocity components), and about the external magnetic field [27, 28].

It is very important to underline that the SC attitude dynamics as the angular motion of rigid bodies systems under the action of external torques was and still is one of the most interesting parts of the classical mechanics. By this reason, it is possible to characterize the presented research as a continuation of the development of fundamental problems of classical dynamics. In this connection, it is worth to indicate, that in this work the research of the DSSC/gyrostat angular motion under the action of the magnetic restoring torque is fulfilled in the generalized formulation close to the task of the motion of the Lagrange top [1-6] with obtaining analytical exact solutions for the motion parameters in terms of elliptic integrals and the Jacobi functions.

1. Mechanical and mathematical models

As previously mentioned, the magnetic actuators of the SC produce the magnetic dipole moment (**m**), which interacts with the Earth's magnetic field (with the vector of the magnetic induction $\mathbf{B}_{orb}$) and generates the corresponded external torque:

$$\mathbf{M}_m = \mathbf{m} \times \mathbf{B}_{orb} \tag{1.1}$$

In this work, we will describe the SC angular motion on a quite short time-interval, which corresponds to a short sector of the trajectory motion of the SC mass center, when the vector of the induction of the Earth's magnetic field $\mathbf{B}_{orb}$ practically does not change its direction and magnitude. In this case we can assume the constancy of the vector of the induction of the Earth's magnetic field in the inertial space $\left(\mathbf{B}_{orb} = \overrightarrow{\text{const}}\right)$.

In this research, the control law for the magnetic actuators is defined by the current values of the angular velocity components. Let us consider the control law, which is tracking the signals from the SC angular velocity sensors and forming the proportional components of the magnetic dipole moment:

$$\mathbf{m} = k\boldsymbol{\omega} \tag{1.2}$$

where $\boldsymbol{\omega}$ is the vector of the SC angular velocity (in the connected SC coordinates frame this vector

has the components $\boldsymbol{\omega} = [p, q, r]^T$), and k – is the constant coefficient. This control law (1.2) can be considered as the particular case of the generically defined control described in [12-15]:

$$\mathbf{u} = \varepsilon^2 k_p \mathbf{q} + \varepsilon k_v \mathbf{I}\boldsymbol{\omega} \tag{1.3}$$

where k_p, k_v, ε are constants; $\mathbf{u}$ is the modified control-vector (corresponding directly to the dipole moment's $\mathbf{m}$ components in the connected SC coordinates frame); $\mathbf{q}$ – is the vector of quaternions; $\mathbf{I}$ – is the SC inertia tensor. By the reason of the proportionality of the dipole moment components to the corresponded components of the angular velocity vector $\boldsymbol{\omega}$, let us call the regime of the angular motion with the dipole moment modulation (1.2) as "*the ω-regime*".

It is very important to note that the SC angular motion under the action of the magnetic torque (1.1) with control law (1.2) in presence of a constant magnetic induction field $\mathbf{B}_{orb}$ is interesting from the side of the SC natural dynamics investigation, and in terms of classical mechanics. The defined case of motion can be characterized as the development of classical tasks of rigid body dynamics. This case is close to the Lagrange top ideology: the external restoring/tilting torque is presented, but with the complex modulation of the torque magnitude (which is proportional to the value of the angular velocity).

As it was indicated above, we intend to consider the attitude dynamics of the SC at the short sector of its orbital motion. In these conditions, it is possible to investigate the angular motion of the SC around the center of mass C (fig.1) under the action of the external torque created by the interaction between the SC own magnetic dipole moment (1.2) and the external magnetic field with the constant magnetic induction $\mathbf{B}_{orb}$, which defines the "selected" direction (the axis CZ) in the inertial space, described by the main inertial frame of coordinates $CXYZ$. The angular position of the SC and its connected coordinates frame $Cxyz$ relatively the selected inertial direction CZ is described by the well-known directional cosines: $\gamma_1 = \cos(CZ, Cx)$, $\gamma_2 = \cos(CZ, Cy)$, $\gamma_3 = \cos(CZ, Cz)$.

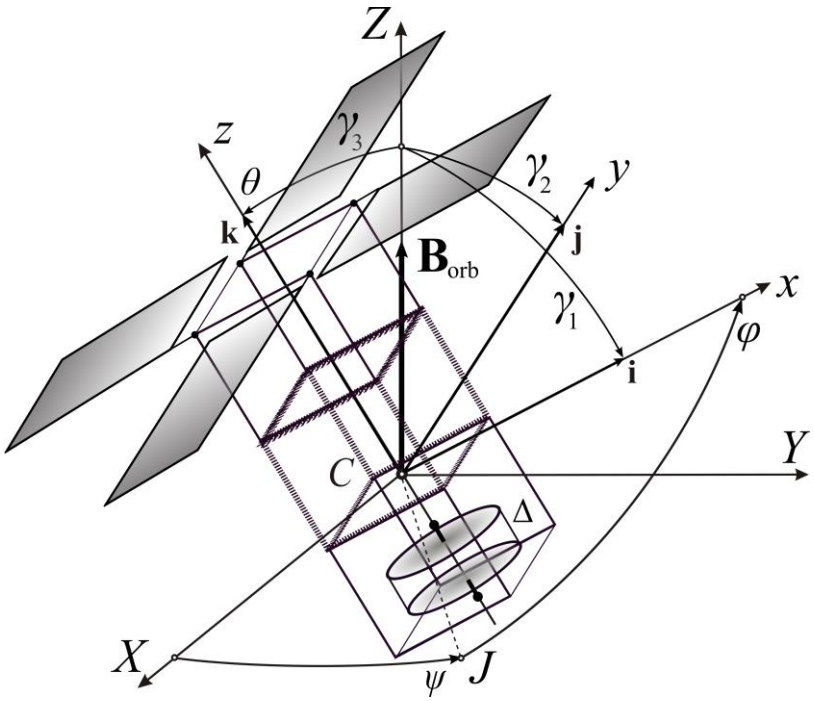

Fig.1 – *The DSSC schematic construction and coordinates systems*

Then the magnetic induction vector and the magnetic dipole moment will have the following components in the body-fixed reference frame *Cxyz*:

$$\mathbf{B}_{orb} = B_{orb}\left[\gamma_1, \gamma_2, \gamma_3\right]^T; \quad \mathbf{m} = k\left[p, q, r\right]^T \tag{1.4}$$

Using (1.1) and composing vectors (1.4), let us write the dynamical equations [6-9] of the DSSC (fig.1) and the kinematical equations for directional cosines of the *CZ* axis relatively the direction of the constant vector $\mathbf{B}_{orb}$:

$$\begin{cases} A\dot{p} + \left(C_b - A\right)qr + q\Delta = kB_{orb}\left(q\gamma_3 - r\gamma_2\right) \\ A\dot{q} + \left(A - C_b\right)pr - p\Delta = kB_{orb}\left(r\gamma_1 - p\gamma_3\right) \\ C_b\dot{r} + \dot{\Delta} = kB_{orb}\left(p\gamma_2 - q\gamma_1\right) \\ \dot{\Delta} = M_\Delta \end{cases} \tag{1.5}$$

$$\begin{cases} \dot{\gamma}_1 = r\gamma_2 - q\gamma_3 \\ \dot{\gamma}_2 = p\gamma_3 - r\gamma_1 \\ \dot{\gamma}_3 = q\gamma_1 - p\gamma_2 \end{cases} \tag{1.6}$$

where $A = A_b + A_r$, $C = C_b + C_r$; $\left\{A_b, A_b, C_b\right\}$ are the axial inertia moments of the dynamically symmetrical main SC's body in the connected frame; $\left\{A_r, A_r, C_r\right\}$ are the axial inertia moments of the dynamically symmetrical rotor in its own connected frame; $M_\Delta -$ is the internal torque acting on the rotor from the side of the main body. Here we also note the connections between the directional cosines and the Euler angles (as we can see, the precession angle ψ is not involved in the dynamics):

$$\begin{cases} \gamma_1 = \sin\theta\sin\varphi \\ \gamma_2 = \sin\theta\cos\varphi \\ \gamma_3 = \cos\theta \end{cases} \tag{1.7}$$

In this research we will consider the dynamics of our coaxial SC (the main body and the rotor) at the absence of theirs interaction (M_Δ=0) and, therefore, everywhere below Δ=const.

2. The first integrals of the motion

For the considered case four conservation laws hold. Firstly, the constant value of the *CZ*-unit-vector gives the trivial first integral (the conservation law):

$$\gamma_1^2 + \gamma_2^2 + \gamma_3^2 = 1 \tag{2.1}$$

Secondly, the projection of the angular momentum of the system on the "selected" axis *CZ* are

constant by the reason of the absence of corresponding projections of external torques (1.1):

(2.2) $$Ap\gamma_1 + Aq\gamma_2 + \left(C_b r + \Delta\right)\gamma_3 = K_Z = \text{const}$$

The third integral follows from the combination of dynamical equations (1.5) (thus, the first equation from (1.5) is multiplied by *p*, the second – by *q*, the third – by *r*, and the corresponding results are summarized and integrated):

(2.3) $$A\left(p^2 + q^2\right) + C_b r^2 = h = \text{const}$$

The fourth (last) integral can be simply obtained: as can we see, from the third equation (1.5) and the last equation (1.6) the expression follows:

(2.4) $$\frac{d}{dt}\left(C_b r + \Delta\right) = kB_{orb}\left(-\dot{\gamma}_3\right)$$

and after the integration we obtain

(2.5) $$C_b r + \Delta = -kB_{orb}\gamma_3 + D$$

where *D* is the constant defined by the initial conditions. The same result in the revised form can be presented as the last "first" integral:

(2.6) $$C_b r^2 = \frac{1}{C_b}\left[D - kB_{orb}\gamma_3 - \Delta\right]^2$$

Also the important identity can be written with the help of regular transformations [1], taking into account the expression (2.1):

(2.7) $$\left(p\gamma_1 + q\gamma_2\right)^2 + \left(q\gamma_1 - p\gamma_2\right)^2 = \left(p^2 + q^2\right)\left(\gamma_1^2 + \gamma_2^2\right) = \left(p^2 + q^2\right)\left(1 - \gamma_3^2\right)$$

So, the found first integrals and the identity (2.1)-(2.7) allow to find the analytical solutions for the motion dynamical parameters, including explicit time-dependencies for the angular velocity components and for kinematical parameters (the directional cosines and/or the Euler angles).

3. The obtainment of the exact explicit solutions

With the help of the last kinematical equation (1.6), and the first integrals (2.1)-(2.6) we can rewrite the expression (2.7) in the form of the differential equation:

(3.1) $$\frac{1}{A^2}\left[K_Z-\left(C_b r+\Delta\right)s\right]^2+\dot{s}^2=\frac{1}{A}\left(h-C_b r^2\right)\left(1-s^2\right)$$

where the usable designations is involved $s\overset{df}{=}\gamma_3$.

In view of expressions (2.6) and (2.5), the differential equation (3.1) takes the shape:

(3.2) $$\pm\dot{s}=\sqrt{\frac{1}{A}\left(h-\frac{1}{C_b}\left[D-kB_{orb}s-\Delta\right]^2\right)\left(1-s^2\right)-\frac{1}{A^2}\left[K_Z-\left(D-kB_{orb}s\right)s\right]^2}=\sqrt{\mathrm{poly}_4(s)}$$

where $\mathrm{poly}_4(s)$ is the 4th power polynomial, that refers the integral to the elliptical integrals [29-31]:

(3.3) $$\int_{s_0}^{s}\frac{ds}{\sqrt{\mathrm{poly}_4(s)}}=\pm\int_0^t dt=\pm t$$

To write the explicit solution for the *s*-variable in terms of the Jacobi-functions we should invert the elliptic integral (3.3). By this reason, it is needed to fulfill the change of variables:

(3.4) $$s=\frac{\alpha+\beta w}{1+w}$$

where constants α and β (the numerical values) are selected from the requirements of nulling the coefficients of terms of the first and the third powers of the numerator of the recalculated polynomial ($\{p_3, p_1\}\to 0$):

(3.5) $$\mathrm{poly}_4\left(s(w)\right)=\frac{p_4w^4+p_3w^3+p_2w^2+p_1w+p_0}{A^2C_b\left(1+w\right)^4}=\frac{p_4w^4+p_2w^2+p_0}{A^2C_b\left(1+w\right)^4}$$

therefore the values of constants α and β follow from the algebraic system of two polynomial equations:

(3.6) $$\left\{p_1(\alpha,\beta)=0;\quad p_3(\alpha,\beta)=0\right\}\to\left\{\alpha,\beta\right\}$$

The Polynomial (3.5) can be written in a factored form, according to the sign of the coefficient p_4 and the roots $\{X_1, X_2\}$ of the auxiliary quadratic equation $p_4X^2+p_2X+p_0$ (where values of the roots are denoted for the convenience as $X_1=\pm a^2$; $X_2=\pm b^2$). So, the five cases of this factorized form are possible:

(3.7)
$$\left[\begin{array}{l}
1)\ \ p_4<0;\ \ X_1=a^2>0;\ X_2=b^2>0:\quad \mathrm{poly}_4\left(s(w)\right)=\dfrac{|p_4|\left(a^2-w^2\right)\left(w^2-b^2\right)}{A^2C_b\left(1+w\right)^4};\\
2)\ \ p_4<0;\ \ X_1=-a^2<0;\ X_2=b^2>0:\quad \mathrm{poly}_4\left(s(w)\right)=\dfrac{|p_4|\left(w^2+a^2\right)\left(b^2-w^2\right)}{A^2C_b\left(1+w\right)^4};\\
3)\ \ p_4>0;\ \ X_1=a^2>0;\ X_2=b^2>0:\quad \mathrm{poly}_4\left(s(w)\right)=\dfrac{|p_4|\left(w^2-a^2\right)\left(w^2-b^2\right)}{A^2C_b\left(1+w\right)^4};\\
4)\ \ p_4>0;\ \ X_1=-a^2<0;\ X_2=b^2>0:\quad \mathrm{poly}_4\left(s(w)\right)=\dfrac{|p_4|\left(w^2+a^2\right)\left(w^2-b^2\right)}{A^2C_b\left(1+w\right)^4};\\
5)\ \ p_4>0;\ \ X_1=-a^2<0;\ X_2=-b^2<0:\quad \mathrm{poly}_4\left(s(w)\right)=\dfrac{|p_4|\left(w^2+a^2\right)\left(w^2+b^2\right)}{A^2C_b\left(1+w\right)^4}
\end{array}\right.$$

The forms of the polynomial factorizations (3.7) define the cases of the elliptic integral (3.3) inversion after the transition to the new variable *w*:

(3.8)
$$\int\limits_{s_0}^{s}\frac{ds}{\sqrt{\mathrm{poly}_4(s)}}=\int\limits_{w_0}^{w}\frac{\left(\beta-\alpha\right)dw}{\left(1+w\right)^2\sqrt{\mathrm{poly}_4\left(s(w)\right)}}=\pm t$$

So, the integral (3.8) invertion in the first case (3.7)-1) can be implemented in the form:

$$\int\limits_{w_0}^{w}\frac{\left(\beta-\alpha\right)dw}{\left(1+w\right)^2\sqrt{\mathrm{poly}_4\left(s(w)\right)}}=-\left[\int\limits_{w}^{a}+\int\limits_{a}^{w_0}\right]\left(\frac{\beta-\alpha}{\left(1+w\right)^2\sqrt{\dfrac{|p_4|\left(a^2-w^2\right)\left(w^2-b^2\right)}{A^2C_b\left(1+w\right)^4}}}\right)dw=\pm t$$

or

(3.9)
$$\int\limits_{w}^{a}\frac{a\,dw}{\sqrt{\left(a^2-w^2\right)\left(w^2-b^2\right)}}=\frac{\mp a\sqrt{|p_4|}}{\left(\beta-\alpha\right)\sqrt{A^2C_b}}t-J_0;\qquad J_0=\int\limits_{a}^{w_0}\frac{a\,dw}{\sqrt{\left(a^2-w^2\right)\left(w^2-b^2\right)}}=\mathrm{const}$$

In this form (3.9) the elliptic integral is immediately inversed [29] to the dn(*x*|*m*) elliptic function:

(3.10)
$$w=a\,\mathrm{dn}\left(x\,|\,m\right);\quad x=\frac{\mp a\sqrt{|p_4|}}{\left(\beta-\alpha\right)\sqrt{A^2C_b}}t-J_0;\quad m=\sqrt{\frac{a^2-b^2}{a^2}};\quad \left(or\quad \tilde{m}=\frac{a^2-b^2}{a^2}\right)$$

Returning to the natural variable γ_3, we finally obtain the main exact analytical solution (for the nutation angle):

(3.11) $$\cos\theta = s = \gamma_3(t) = \frac{\alpha + \beta a\,\mathrm{dn}\left(x(t)\,|\,m\right)}{1 + a\,\mathrm{dn}\left(x(t)\,|\,m\right)}$$

To confirm the main exact solution (3.11) we can present the comparative results of the differential equations (1.5) and (1.6) numerical integration (the line), and the formula (3.11) evaluation (dots), that is depicted at the figure (fig.2). Simultaneously, in addition to the fig.2, it is important to present the numerical integration results for all of the dynamical parameters. The hypothetical numerical parameters for calculations (fig.2, 3) are following: A_b=12, B_b=12, C_b=6, A_r=10, C_r=6 [kg·m^2]; p_0=0.4, q_0=0.0, r_0=0.1 [rad/s]; Δ=1 [kg·m^2/s]; γ_{10}=0.6, γ_{20}=0.6, γ_{30}=0.5292; kB_{orb}=-8 [N·m·s]; K_Z=6.1266, D=-2.6332 [kg·m^2/s]; h=3.58 [kg·m^2/s^2].

Then the following concretized algebraic equations (3.6) are actual:

$$\begin{cases} p_1 = \left(4096.00\alpha^3 - 3078.2992\alpha^2 - 2087.2031\alpha + 1085.2949\right)\beta - \\ -1026.0997\alpha^3 - 2087.2031\alpha^2 + 3255.8848\alpha - 172.2312 = 0; \\ \\ p_3 = \left(4096.00\beta^3 - 3078.2992\beta^2 - 2087.2031\beta + 1085.2949\right)\alpha - \\ -1026.0997\beta^3 - 2087.2031\beta^2 + 3255.8848\beta - 172.2312 = 0; \end{cases}$$

with the solutions α=-0.3011, β=0.9933 (one of the possible), and polynomial (3.5) coefficients: p_4=-3.4805; p_2=3306.8803; p_0=-428.0900, and its corresponding roots: X_1=0.1295; X_2=949.9867. Then the elliptic module and defined integral are m=0.9999 and J_0=-3.5494; we can consider this case as the interesting extreme case (fig.2, 3) with the elliptic module close to the unit value.

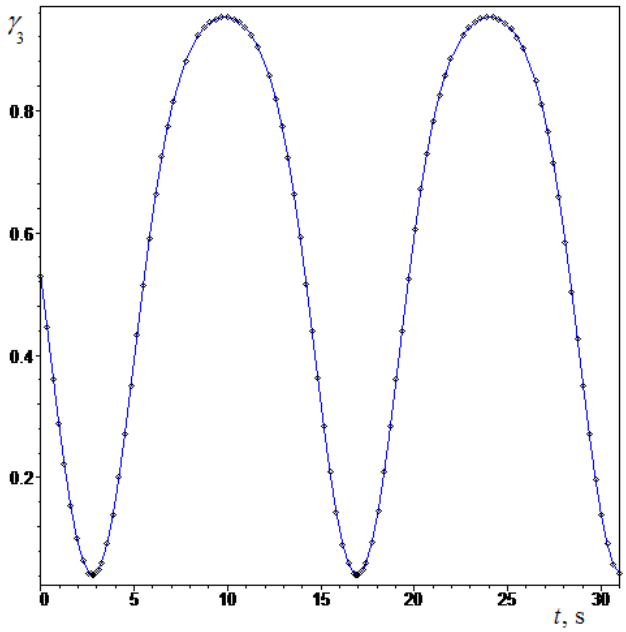

Fig.2 – *The comparative modelling results for* $\gamma_3(t)$:
the line – the numerical integration; dots – the analytical solution (3.11)

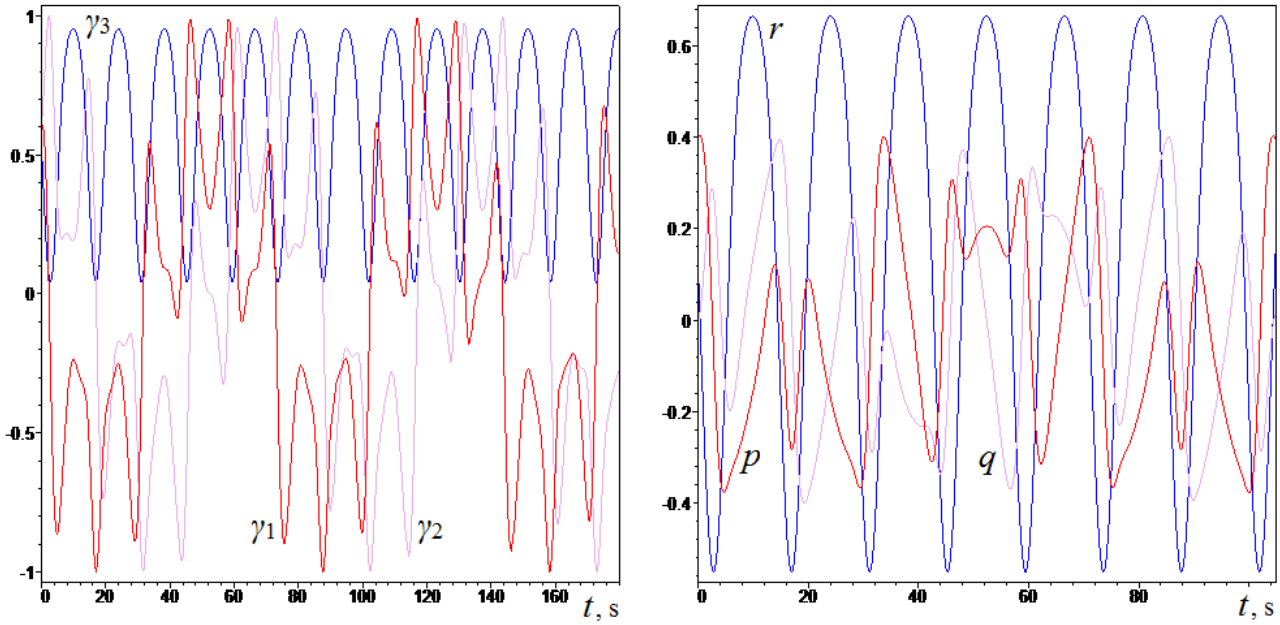

Fig.3 - *Results of the numerical calculations*

For the other cases (3.7)-2) – (3.7)-5) the analytical solutions can be obtained by analogy:

(3.12)

$$\left[\begin{array}{l}
2)\ w=b\,\mathrm{cn}\left(x\,|\,m\right);\ x=\dfrac{\mp\sqrt{a^2+b^2}\sqrt{|p_4|}}{\left(\beta-\alpha\right)\sqrt{A^2C_b}}t-J_0;\ m=\sqrt{\dfrac{b^2}{a^2+b^2}};\ J_0=\displaystyle\int_b^{w_0}\dfrac{a\,dw}{\sqrt{\left(w^2+a^2\right)\left(b^2-w^2\right)}};\\
3)\ w=b\,\mathrm{sn}\left(x\,|\,m\right);\ x=\dfrac{\pm a\sqrt{|p_4|}}{\left(\beta-\alpha\right)\sqrt{A^2C_b}}t-J_0;\ m=\sqrt{\dfrac{b^2}{a^2}};\ J_0=\displaystyle\int_{w_0}^{0}\dfrac{a\,dw}{\sqrt{\left(w^2-a^2\right)\left(w^2-b^2\right)}};\\
4)\ w=b\,\mathrm{nc}\left(x\,|\,m\right);\ x=\dfrac{\pm\sqrt{a^2+b^2}\sqrt{|p_4|}}{\left(\beta-\alpha\right)\sqrt{A^2C_b}}t-J_0;\ m=\sqrt{\dfrac{a^2}{a^2+b^2}};\ J_0=\displaystyle\int_{w_0}^{b}\dfrac{a\,dw}{\sqrt{\left(w^2+a^2\right)\left(w^2-b^2\right)}};\\
5)\ w=b\,\mathrm{sc}\left(x\,|\,m\right);\ x=\dfrac{\pm a\sqrt{|p_4|}}{\left(\beta-\alpha\right)\sqrt{A^2C_b}}t-J_0;\ m=\sqrt{\dfrac{a^2-b^2}{a^2}};\ J_0=\displaystyle\int_{w_0}^{0}\dfrac{a\,dw}{\sqrt{\left(w^2+a^2\right)\left(w^2+b^2\right)}};
\end{array}\right.$$

where the classical elliptic Jacobi functions take place: cn(·) – the elliptic cosine, sn(·) – the elliptic sinus, nc(·)=1/cn(·), sc(·)=sn(·)/cn(·).

Now, from the expression (2.5) it is possible to obtain the function $r(t)$ as the already found analytical solution:

(3.13)
$$r\left(t\right)=\left[-kB_{orb}\gamma_3\left(t\right)+D-\Delta\right]/C_b$$

Let us to change the variables for the equatorial components of the angular velocity:

(3.14)
$$p=G\cos F;\quad q=G\sin F$$

Then from the energy integral (2.3) we will have for the amplitude of the equatorial velocity the exact value:

$$G(t) = p^2 + q^2 = \left[h - C_b r^2(t)\right] / A \tag{3.15}$$

It is easy to write the identity [1]:

$$p\dot{q} - q\dot{p} = \left(p^2 + q^2\right)\dot{F} \tag{3.16}$$

From the first and the second equations (1.5) the expression follows:

$$A\left(p\dot{q} - q\dot{p}\right) = \left[\Delta - \left(A - C_b\right)r - kB_{orb}\gamma_3\right]\left(p^2 + q^2\right) + kB_{orb}r\left(p\gamma_1 + q\gamma_2\right) \tag{3.17}$$

From the first integral (2.2) the expression can be found:

$$p\gamma_1 + q\gamma_2 = \left[K_Z - \left(C_b r + \Delta\right)\gamma_3\right] / A \tag{3.18}$$

Taking in view the expressions (3.16)-(3.18), the differential equation can be constituted:

$$\dot{F} = \frac{1}{A}\left[\Delta - \left(A - C_b\right)r(t) - kB_{orb}\gamma_3(t)\right] + \frac{kB_{orb}r(t)\left[K_Z - \left(C_b r + \Delta\right)\gamma_3(t)\right]}{A\left[h - C_b r^2(t)\right]} \tag{3.19}$$

From the equation (3.19) the formal exact explicit quadrature follows:

$$F(t) = \int\left(\frac{1}{A}\left[\Delta - \left(A - C_b\right)r(t) - kB_{orb}\gamma_3(t)\right] + \frac{kB_{orb}r(t)\left[K_Z - \left(C_b r(t) + \Delta\right)\gamma_3(t)\right]}{A\left[h - C_b r^2(t)\right]}\right)dt + \text{const} \tag{3.20}$$

Here it is important to note, that in the integral (3.20) the integration of elliptic functions is fulfilled, and the corresponding result of integration can be expressed in terms of the theta-functions [29] (in this work we will not obtain the final explicit expressions for this result).

The expressions (3.20) and (3.15) fully define the analytical solutions for the angular velocity equatorial components $p(t)$ and $q(t)$.

The analytical solution for $\gamma_3(t)$ (e.g. (3.11)) allows to consider (after differentiating by time) the last differential equation (1.6) as the algebraic equation. Adding to this algebraic equation the expression (3.18), we take the complete linear algebraic system of equations relative the $\gamma_1(t)$ and $\gamma_2(t)$:

$$\begin{cases} q(t)\gamma_1 - p(t)\gamma_2 = \dfrac{d}{dt}\left(\dfrac{\alpha + \beta a\,\mathrm{dn}\left(x(t)\,|\,m\right)}{1 + a\,\mathrm{dn}\left(x(t)\,|\,m\right)}\right); \\ p(t)\gamma_1 + q(t)\gamma_2 = \left[K_Z - \left(C_b r(t) + \Delta\right)\gamma_3(t)\right] / A; \end{cases}$$

which allows to write the final analytical solutions for the $\gamma_1(t)$ and $\gamma_2(t)$:

$$(3.21)\quad \begin{cases} \gamma_1 = \dfrac{1}{q(t)}\dfrac{d}{dt}\left(\dfrac{\alpha+\beta a\,\mathrm{dn}\left(x(t)\,|\,m\right)}{1+a\,\mathrm{dn}\left(x(t)\,|\,m\right)}\right)+\dfrac{p(t)}{q(t)}\gamma_2; \\ \gamma_2 = \left[\left[K_Z-\left(C_b r(t)+\Delta\right)\gamma_3(t)\right]/A-\dfrac{p(t)}{q(t)}\dfrac{d}{dt}\left(\dfrac{\alpha+\beta a\,\mathrm{dn}\left(x(t)\,|\,m\right)}{1+a\,\mathrm{dn}\left(x(t)\,|\,m\right)}\right)\right]\Bigg/\left[\dfrac{p^2(t)}{q(t)}+q(t)\right]. \end{cases}$$

So, the time-dependencies for the all dynamical parameters of the system at the realization of the ω-regime are written in exact analytical form, and the considered task is fully solved. The obtained exact expressions can be applied not only to the analysis, but also to the parametrical synthesis of the DSSC motion dynamics at the implementation of the ω-regime.

4. Using the ω-regime in tasks of the spacecraft attitude dynamics and control

The analytical solutions from the previous section can be used for the design of a new scheme of the attitude reorientation of the dual-spin spacecraft (gyrostat-satellite). As we will see below, the ω-regime is the quite simple way to reorient the longitudinal axis of the DSSC strongly along the direction of the angular momentum vector starting from the arbitrary direction. This reorientation of the DSSC axis corresponds to the transition of the DSSC to its ideal spin-stabilized spatial position – this is the most appropriate passive dynamics of the DSSC with its preferable attitude.

4.1. The main idea and the algorithm of the DSSC reorientation

To construct the algorithm of the spacecraft reorientation into the stabilized direction along the angular momentum vector, it is worthwhile to recall the properties of the torque-free motion of a symmetrical rigid body (spacecraft) around its center of mass. As it is well known, in the free motion the longitudinal component of the angular velocity $r(t)$ will be constant. In addition, a constant value retains for the nutation angle $\bar{\theta}(t)$ evaluated relatively the direction of the vector of the angular momentum (**K**) of the free motion:

$$(4.1)\qquad r(t)=\bar{r}=\mathrm{const};\qquad \cos\bar{\theta}(t)=\bar{\gamma}_3(t)=\frac{C_b\bar{r}+\Delta}{K}=\mathrm{const}$$

The idea of the spatial reorientation using the ω-regimes is based on the alternation of intervals of the motion with switched on ω-regimes and intervals of the free motion (with switched off all magnetic torques). Here, as we will show, to fulfill the spatial reorientation of the longitudinal axis strongly along the angular momentum vector it is needed to create the ω-regimes in the corresponding time-intervals when the time-dependence of the angular velocity component $r(t)$ has the half-period of the increase of its magnitude, evaluated by the solution (3.13). Let us call these time-intervals as the "growth intervals" (magenta columns at the fig.4); and the dynamics of the spacecraft on such alternating intervals we will call as the "growing dynamics".

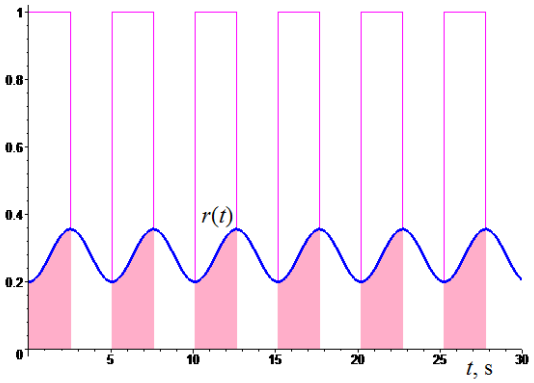

Fig.4 – *The "growth intervals" with the increase of the r(t)-value by the solution* (3.13)

The time-history of the DSSC dynamical parameters at the implementation of the "growing dynamics" is depicted in the figure (fig.5). The graphics (fig.5) are obtained by the numerical integration of the dynamical equations with the impulsive actuation of the magnetic dipole (1.4) on the "growth intervals".

Between the growth intervals (where the magnetic torques are disabled) the angular velocity component $r(t)$ is constant because the motion here is free. The same dynamical behavior has the directional cosines $\overline{\gamma}_3(t)$ evaluated relatively the current angular momentum vector (it changes its direction and magnitude passing through growth intervals). We can see the coincidence of dynamical behaviors of the time-dependences $r(t)$ and $\overline{\gamma}_3(t)$ in the qualitative sense (fig.5).

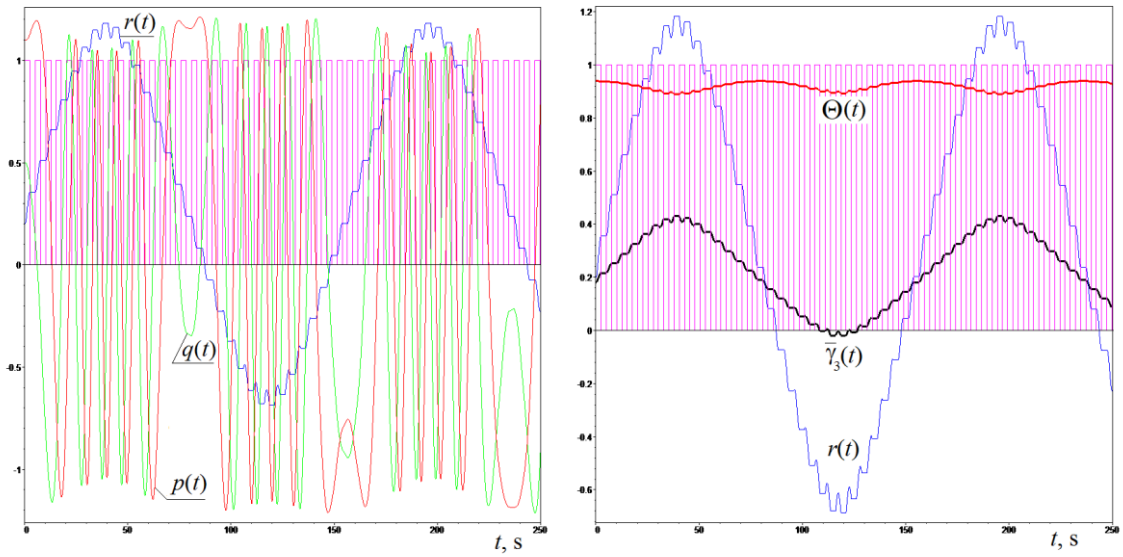

Fig. 5 – *The dynamical parameters of the spacecraft in the "growing dynamics"*

As it follows from modeling results (fig.5), the growing dynamics allows to change values of $r(t)$ and $\overline{\gamma}_3(t)$ passing through the growth intervals. This change of the dynamical parameters we can use to reorient of the spacecraft, starting from the one regime of free motion and finalizing in the another one.

Moreover, the first step of the growing dynamics (the first initiated ω-regime) always inevitably leads to increasing the $r(t)$-value, because the growth intervals are selected using the analytical solution (3.13) as the time-intervals which exactly provide the half-period of increasing the $r(t)$-magnitude. From the modelling (fig.5) results the confirmation of increasing the $r(t)$ magnitude follows not only in the first growth interval, but also in the next few steps. Nevertheless, after the increase of the $r(t)$-value in few growth intervals, the backward evolution with decreasing the $r(t)$-value is realized in the following steps. This dynamical evolution can be explained by the magnification of differences between the current values of the dynamical parameters (continuously changing during the passage through the alternating regimes) and their predefined analytical values (and first of all, the elliptic module m value changing the period of oscillations). In any case, the first growth intervals are applicable to increasing the $r(t)$-value and, therefore, to increasing the $\bar{\gamma}_3(t)$ – this corresponds to the improvement of the current attitude of the spacecraft, since the longitudinal axis of the DSSC has become closer to the direction of the vector of the angular momentum. Also it is possible to note the synchronous evolution (fig.5) of the direction of the angular momentum vector relatively the "vertical" axis CZ, which is described by the angle $\Theta = \angle(CZ, \mathbf{K})$.

So, this properties of the attitude evolution during the stepwise creation of ω-regimes can be used to the complete attitude reorientation of the DSSC along the angular momentum vector by the way of the initiation of several series of the "growing dynamics" at the recalculation of values of growth intervals period by the analytical solution for the each series.

First of all, we should define the period of the current stepwise ω-regime. From the analytical solutions (3.13) and (3.11) it easy to obtain the full period of dynamical parameters using the known properties of the elliptic functions including the information about periods and poles [29]:

Table 1

	Pole iT′	Pole T+iT′,	Pole T	Pole 0
Half-period iT′	sn s	cd s	dc s	ns s
Half-period T+iT′	cn s	sd s	nc s	ds s
Half-period T	dn s	nd s	sc s	cs s

The real and imaginary "quarter-periods" T and T′ [29] correspond to the complete elliptic integrals of the first kind:

$$\text{(4.2)} \qquad \mathrm{T} = \mathrm{T}(m) = \int_0^1 \frac{dw}{\sqrt{(1-w^2)(1-mw^2)}} = \int_0^{\pi/2} \frac{d\xi}{\sqrt{(1-m\sin^2\xi)}}; \qquad \mathrm{T}' = \mathrm{T}(1-m)$$

Due to describing the real motion of the spacecraft, it is necessary to use only real part of the elliptic functions. Then, as it follows from the solution (3.10) at the obtained value of the elliptic parameter m the period of the function $s(t)$ is equal to 2T. This value T allows to create the correct impulsive actuation of the ω-regime on the corresponded series of growth intervals (fig.4) at the evaluated m and initial phase J_0 (3.9).

In purposes of practical implementation of the considered impulsive technique of the growing dynamics, we can suggest the universal scheme with only one (only first) growth interval for each series of impulses (i.e. the single-impulse-series). Then the algorithm of the DSSC attitude reorientation will have the following structure (fig.6).

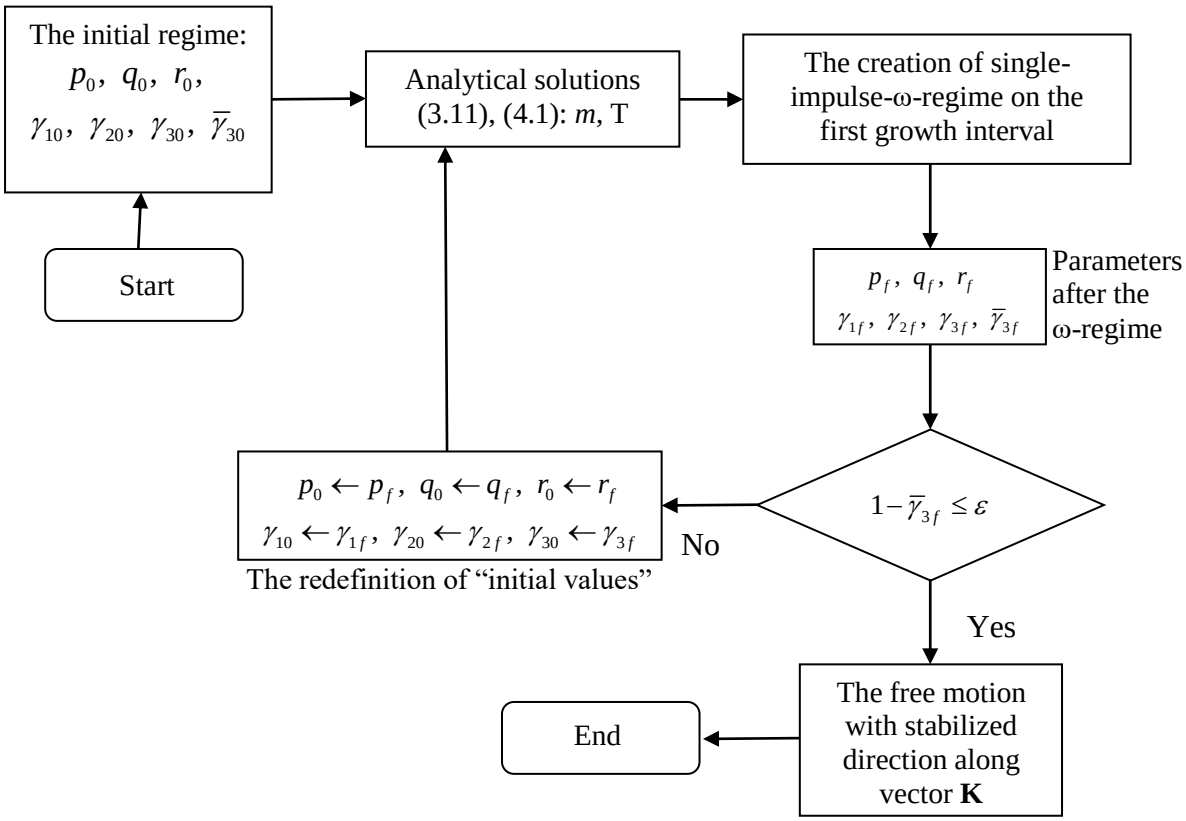

Fig.6 – *The algorithm of the spacecraft reorientation using series of single-impulse-ω-regimes*

The main condition checked at the each step of the algorithm is the obtainment of the spatial position along the vector of the angular momentum $(\overline{\gamma}_3 = 1)$ with the predefined accuracy value $\varepsilon << 1$. The implementation of this technique will be considered in the next section, where the confirming modeling results are presented.

4.2. The reorientation algorithm numerical modeling

As previously mentioned, the reorientation idea is based on the alternating regimes of the torque-free motion and the ω-regimes on the growth intervals. In the case of the universal algorithm (fig.6) only one (the first) growth interval is recommended, where we have the fully correct correspondence of the current motion parameters (which are considered as the initial values for the analytical solutions) and parameters of the ω-regime (which are calculated by the analytical solutions). However, for the rapid demonstration of the idea in the framework of subsequent numerical modeling, let us use more than one growth intervals, that, certainly, impairs the right correspondence between the current motion parameters and parameters of the ω-regime for each following interval from the current series.

At the figures (fig.7, 8, 9) nine consistent series of the growing dynamics are presented for the case of small micro/nano-spacecraft. Each fragment of the figure contains time-interval of 100 seconds, where only some of initial growth intervals are active (depicted as magenta columns), and other time corresponds to the torque-free motion of DSSC. It is possible to see from these figures that the $r(t)$-component and $\bar{\gamma}_3(t)$ – value increase their magnitudes on each next series of growth intervals.

We used the following common parameters for all numerical calculations (fig.5-9): A_b=0.13, B_b=0.13, C_b=0.05, A_r=0.05, C_r=0.02 [kg·m^2]; Δ=0.03 [kg·m^2/s]; kB_{orb}=0.005 [N·m·s]. These values are quite applicable to the examination of the hypothetical qualitative dynamics of small DSSC in the geomagnetic field in the case of the angular motion of micro/nano-spacecraft along the low orbit (B_{orb}~50 [μT]) with powerful magnetic torquers ($|\mathbf{m}| = k|\boldsymbol{\omega}| \sim 50 \div 150$ [A·m^2]). The initial conditions and modeling parameters of the series of the ω-regimes are presented the table (tabl.2).

Table 2 – *The modeling parameters*

Fig.7-9	p_0 [1/s]	q_0 [1/s]	r_0 [1/s]	γ_{10}	γ_{20}	γ_{30}	m	J_0	T [s]
(1)	1.1	0.5	0.2	0.387	0.2	0.9	0.861	-0.018	2.141
(2)	0.885	-0.547	1.183	0.258	-0.964	-0.061	0.859	-1.408	2.136
(3)	-0.002	-0.877	1.590	-0.623	-0.338	0.705	0.855	-0.698	2.124
(4)	0.537	0.454	1.875	0.968	0.115	0.224	0.846	-1.504	2.099
(5)	-0.221	0.498	2.056	-0.695	0.626	0.353	0.826	-1.636	2.051
(6)	-0.216	0.222	2.225	0.188	-0.017	0.982	0.738	-0.167	1.893
(7)	0.078	-0.136	2.282	0.028	0.297	0.955	0.637	-0.276	1.781
(8)	-0.069	0.039	2.296	-0.498	-0.080	0.864	0.608	-1.434	1.757
(9)	-0.027	-0.007	2.301	0.282	-0.310	0.908	0.462	-1.134	1.667

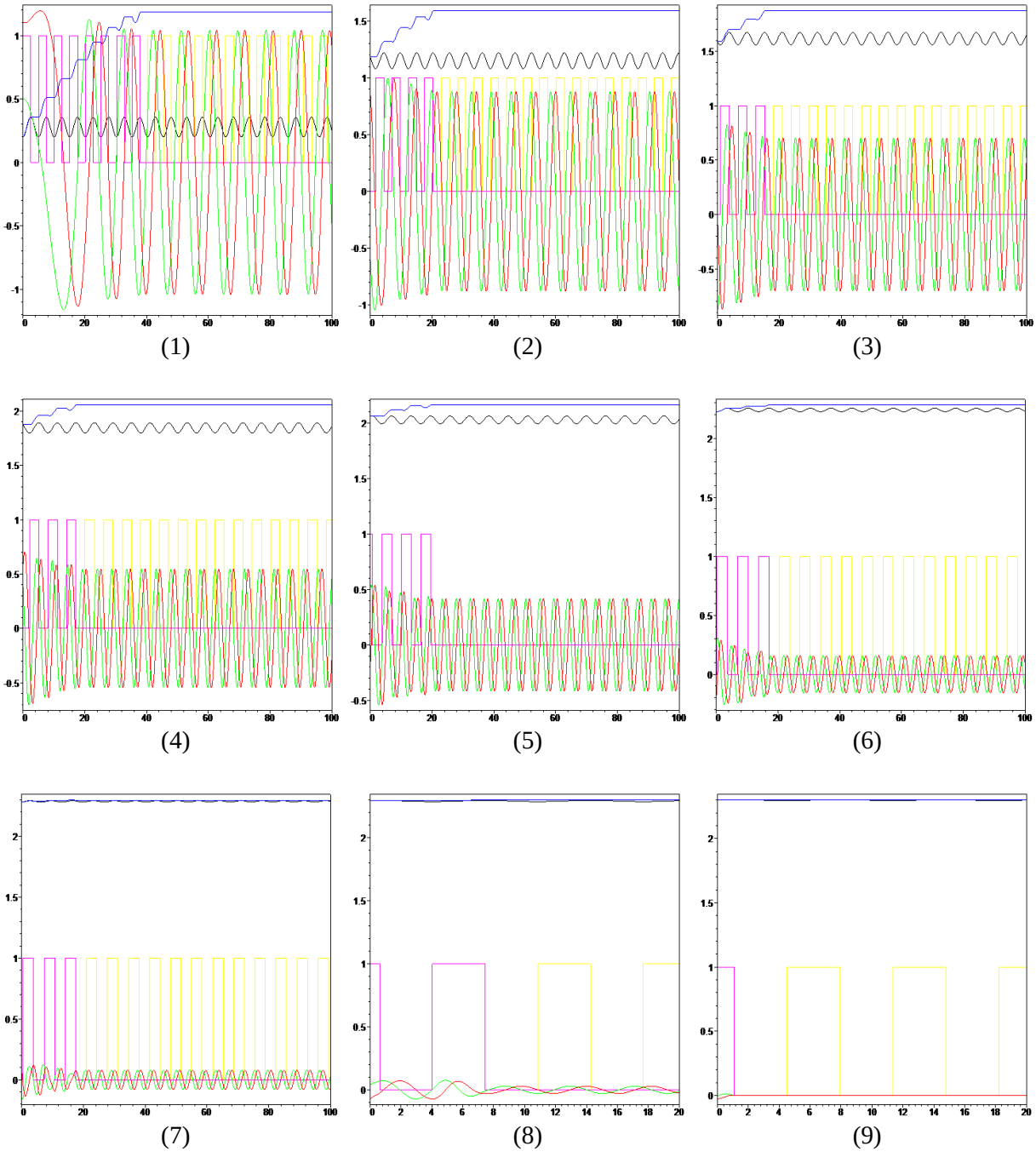

Fig.7 – *The modeling results for the time-history of angular velocity components*:
$p(t)$ – red; $q(t)$ – green; $r(t)$ – blue; magenta columns – the implemented growth intervals;
yellow - inactive growth intervals; black line – the analytical solution (3.13)

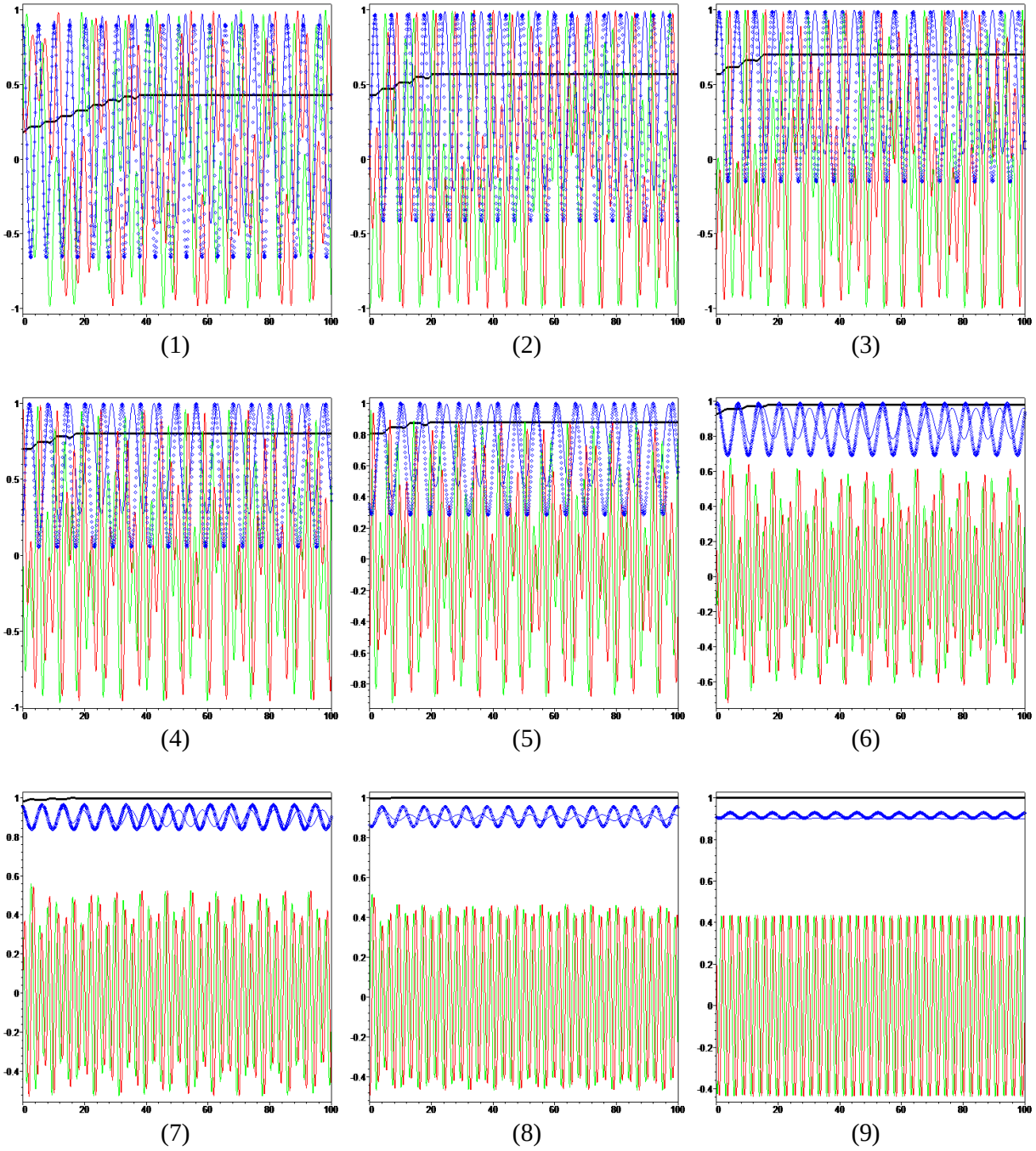

Fig.8 – *The modeling results for the time-history of directional cosines*:
$\gamma_1(t)$ – red; $\gamma_2(t)$ – green; $\gamma_3(t)$ – blue; $\overline{\gamma}_3(t)$ – black; blue dots – the analytical solution (3.11)

It is worth to show separately the first and the last series of the growing dynamics (fig.9). As can we see, the stepwise saturated increase of the *r*(*t*)-component starting from small initial value (fig.9-a) and finishing on the maximal saturated level (fig.9-b) at zero-values of *p*(*t*)- and *q*(*t*)-components of the angular velocity. Also the supreme increase of the $\overline{\gamma}_3(t)$ – value is realized, starting from small value (fig.9-c) and finishing on the level $\overline{\gamma}_3(t) = 0.99999$. Such parameters evolutions mean the fully implementation of the correct reorientation of the DSSC from the "arbitrary" initial spatial position into the final target attitude at the coincidence of the longitudinal axis *Cz* of the DSSC with the

direction of the system angular momentum (realized with the accuracy $\varepsilon=10^{-5}$). Herewith, the vector of the angular momentum is getting closer to the "vertical" vector $\mathbf{B}_{orb}$ in the passages through these series of ω-regimes (from (fig.9-e) to (fig.9-f)).

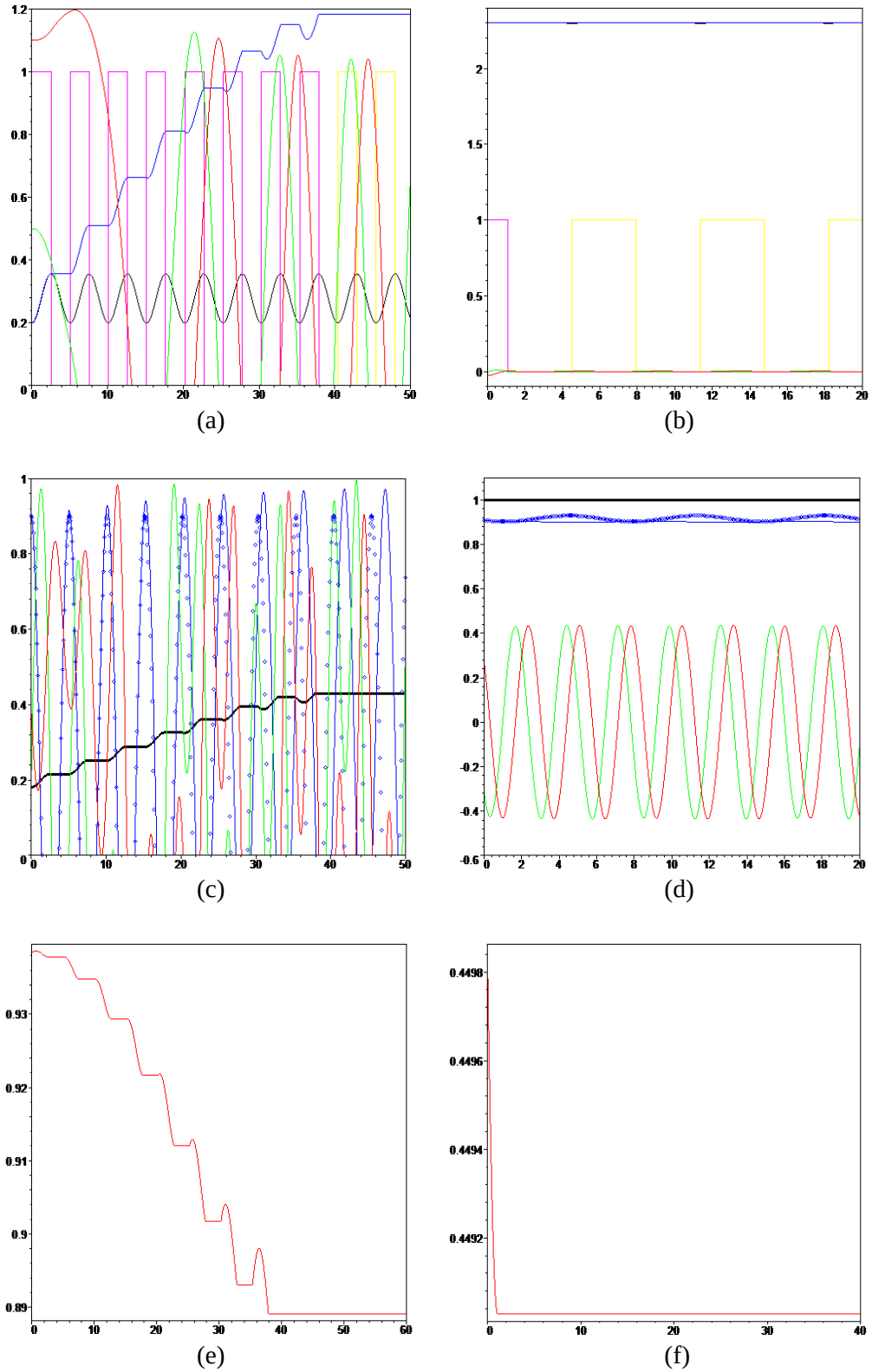

Fig.9 – *The parameters evolution from the first to the last series of* ω*-regimes*:
(a), (b) – the angular velocity components; (c), (d)- directional cosines; (e), (f) – the Θ-evolution

So, the numerical modeling showed the correct implementation of the suggested stepwise algorithm of the DSSC reorientation along the vector of the angular momentum using the series of growth intervals with analytically predefined parameters of each ω-regime. This algorithm is based on the continuous transition through the alternating intervals of the torque-free angular motion and the motion in the ω-regimes. During this transition the magnitudes of the $p(t)$- and $q(t)$-components reduce to the zero-value (it corresponds to the final absence of the equatorial rotation of the DSSC); the longitudinal component of the angular velocity $r(t)$ takes its final supreme magnitude and the longitudinal DSSC axis *Cz* coincides with the direction of the angular momentum vector $\left(\bar{\gamma}_3(t)=1\right)$. Thus, this stepwise algorithm leads to the complete dissipation of the transversal component of the angular velocity at the mechanical energy transfer into the rotation of DSSC about its longitudinal axis; as the result, the DSSC longitudinal axis will be strongly located along the direction of the angular momentum vector.

Conclusion

In this work, the attitude dynamics of dual-spin spacecraft and gyrostat-satellites is considered under the action of magnetic control system. The motion was studied in the constant external magnetic field and at the omega-regime implementation, when the control system forms the spacecraft magnetic dipole moment proportionally to the angular velocity vector. The analytical solutions for all dynamical parameters in terms of elliptic integrals and the Jacobi functions are most important result in the framework of the DSSC attitude dynamics. These new analytical solutions can be characterized as the results developing the classical fundamental problem of the rigid body and gyrostat motion around fixed point. Together with the analytical research, the control algorithm for the angular reorientation of DSSC using the omega-regime was constructed. This algorithm allows to reorient the longitudinal axis of the spacecraft along the angular momentum vector – such attitude is the most preferred spatial position of gyroscopically stabilized satellites, including dual-spin spacecraft and gyrostats. So, the fulfilled analytical investigation and the suggested technical application can be quite actual in the tasks of space-flight dynamics of small spacecraft and micro-/nano-satellites.

Acknowledgments

This work is partially supported by the Russian Foundation for Basic Research (RFBR#15-08-05934-A), and by the Ministry of education and science of the Russian Federation in the framework of the State Assignments to higher education institutions and research organizations in the field of scientific activity in the project # 9.1616.2017/ПЧ (9.1616.2017/4.6).

References

[1] U.A. Arkhangelskiĭ, Analytical rigid body dynamics. Moscow: Nauka, 1977.

[2] J. Wittenburg, Dynamics of Systems of Rigid Bodies. Stuttgart: Teubner, 1977.

[3] V.V. Kozlov, Methods of qualitative analysis in the dynamics of a rigid body, Gos. Univ., Moscow, 1980.

[4] V.V. Beletsky, A.A. Khentov, Tumbling Motion of a Magnetized Satellite, Nauka, Moscow, 1985.

[5] A.C. Stickler, K.T Alfriend, Elementary magnetic attitude control system (1976) J. Spacecr. Rockets 13 (5) 282–287.

[6] V.S. Aslanov, Prostranstvennoe dvizhenie tela pri spuske v atmosfere (Spatial Motion of a Body at Descent in the Atmosphere), Fizmatlit, Moscow, 2004.

[7] V.S. Aslanov, A.V. Doroshin, Two cases of motion of an unbalanced gyrostat (2006) Mechanics of Solids, vol. 41, no.4, pp. 29-39.

[8] M. Shigehara, Geomagnetic attitude control of an axisymmetric spinning satellite, J. Spacecr. Rockets 9 (6) (1972) 391–398.

[9] M.Y. Ovchinnikov, D.S. Roldugin, V.I. Penkov, Three-axis active magnetic attitude control asymptotical study (2015) Acta Astronautica, 110, pp.279-286.

[10] D.S. Roldugin, P. Testani, Spin-stabilized satellite magnetic attitude control scheme without initial detumbling (2014) Acta Astronautica, 94(1), 446-454.

[11] A. Craig Stickler and K.T. Alfriend, Elementary Magnetic Attitude Control System, Journal of Spacecraft and Rockets, Vol. 13, No. 5 (1976), pp. 282-287.

[12] M. Lovera, A. Astolfi, Spacecraft attitude control using magnetic actuators, Automatica 40 (2004) 1405 – 1414.

[13] V. A. Chobotov, Spacecraft attitude dynamics and control. NASA STI/Recon Technical Report A, 92 (1991).

[14] Nijmeijer, Henk, and Arjan Van der Schaft. Nonlinear dynamical control systems. Springer Science & Business Media (2013).

[15] Clarke, Francis H., Yuri S. Ledyaev, Ronald J. Stern, and Peter R. Wolenski. Nonsmooth analysis and control theory. Vol. 178. Springer Science & Business Media (2008).

[16] E. Silani, M. Lovera, Magnetic spacecraft attitude control: a survey and some new results, Control Engineering Practice 13 (2005) 357–371.

[17] M. Iñarrea, Chaos and its control in the pitch motion of an asymmetric magnetic spacecraft in polar elliptic orbit, Chaos, Solitons & Fractals,Volume 40, Issue 4 (2009) 1637-1652.

[18] A.V. Doroshin, Attitude dynamics of gyrostat-satellites under control by magnetic actuators at small perturbations, Communications in Nonlinear Science and Numerical Simulation 49 (2017) 159–175.

[19] V.A. Bushenkov, M. Yu. Ovchinnikov, G.V. Smirnov, Attitude stabilization of a satellite by magnetic coils, Acta Astronautica, Volume 50, Issue 12 (2002) 721-728

[20] M.Yu. Ovchinnikov, D.S. Roldugin, V.I. Penkov, Asymptotic study of a complete magnetic attitude control cycle providing a single-axis orientation, Acta Astronautica 77 (2012) 48–60

[21] M.Yu. Ovchinnikov, A.A. Ilyin, N.V. Kupriynova, V.I. Penkov, A.S. Selivanov, Attitude dynamics of the first Russian nanosatellite TNS-0, Acta Astronautica, Volume 61, Issues 1 (2007) 277-285.

[22] Yan-Zhu Liua, Hong-Jie Yu, Li-Qun Chen, Chaotic attitude motion and its control of spacecraft in elliptic orbit and geomagnetic field, Acta Astronautica 55 (2004) 487 – 494.

[23] Li-Qun Chen, Yan-Zhu Liu, Chaotic attitude motion of a magnetic rigid spacecraft and its control, International Journal of Non-Linear Mechanics 37 (2002) 493–504.

[24] A.Slavinskis, U.Kvell, E.Kulu, I.Sünter, H.Kuuste, S.Lätt, K. Voormansik, M.Noorma, High spin rate magnetic controller for nanosatellites, Acta Astronautica 95 (2014) 218–226.

[25] F. Bayat H. Bolandi, A.A. Jalali, A heuristic design method for attitude stabilization of magnetic actuated satellites, Acta Astronautica 65 (2009) 1813 –1825.

[26] G. Avanzini and F. Giulietti, Magnetic Detumbling of a Rigid Spacecraft, Journal of Guidance, Control, and Dynamics, Vol. 35, No. 4 (2012), pp. 1326-1334.

[27] Flatley T. et al. A B-dot acquisition controller for the RADARSAT spacecraft //NASA Conference Publication. – NASA, 1997. – C. 79-90.

[28] A. Zavoli, F. Giulietti, G. Avanzini, G.D.Matteis, Spacecraft dynamics under the action of Y-dot magnetic control law, Acta Astronautica 122 (2016) 146–158.

[29] M. Abramowitz, I.A. Stegun. Handbook of mathematical functions: with formulas, graphs, and mathematical tables. Vol. 55. Courier Corporation (1964).

[30] H. Bateman, A.Erdélyi. Higher transcendental functions. Vol. 2. New York: McGraw-Hill (1953).

[31] G.A. Korn, T.M. Korn. Mathematical handbook for scientists and engineers: Definitions, theorems, and formulas for reference and review. Courier Corporation (2000).